mathematics

Article

Modelling and Fault Detection for Specific Cavitation Damage Based on the Discharge Pressure of Axial Piston Pumps

Shiqi Xia [1,*], Yimin Xia [1] and Jiawei Xiang [2]

[1] State Key Laboratory of High Performance Complex Manufacturing, Central South University, Changsha 410017, China; xiaymj@csu.edu.cn
[2] College of Mechanical and Electrical Engineering, Wenzhou University, Wenzhou 325035, China; jwxiang@wzu.edu.cn
* Correspondence: shiqixia@csu.edu.cn

Abstract: Cavitation will increase the leakage and discharge pressure fluctuation of axial piston pumps. In particular, specific cavitation damage may aggravate the pressure impact and performance degradation. The influence of the specific cavitation damage on the discharge pressure is unclear, and the need for fault detection of this damage is urgent. In this paper, we propose a discharge pressure-based model and fault detection methodology for the specific cavitation damage of axial piston pumps. The discharge pressure model with specific damage is constructed using a slender hole. The simulation model is solved through numerical integration. Experimental investigation of cavitation damage detection is carried out. Discharge pressure features in the time domain and frequency domain are compared. The results show that waveform distortions, spectrum energy relocation, generation of new frequencies and sidebands can be used as features for fault detection regarding the specific cavitation damage of axial piston pumps.

Keywords: modelling; fault detection; cavitation damage; discharge pressure; axial piston pump

MSC: 76A02

Citation: Xia, S.; Xia, Y.; Xiang, J. Modelling and Fault Detection for Specific Cavitation Damage Based on the Discharge Pressure of Axial Piston Pumps. *Mathematics* **2022**, *10*, 2461. https://doi.org/10.3390/math10142461

Academic Editors: Maria Luminița Scutaru and Catalin I. Pruncu

Received: 13 June 2022
Accepted: 13 July 2022
Published: 14 July 2022

1. Introduction

Axial piston pumps are key power components of hydraulic systems applied in the industrial equipment and construction machinery [1,2]. They can convert mechanical energy into fluid power energy with a high efficiency and compact structure. The fluid with high pressure and a high flow rate can accomplish the power transmission and energy output in these applications.

Structures of an axial piston pump consist of three main interfaces: the interface between the slipper and a swash plate, the interface between the piston and a cylinder block, and the interface between the cylinder block and a valve plate [3,4]. These interfaces with the oil film work as bearings and sealings in the pump [5]. The output flow and pressure of piston pumps are discontinuous and fluctuate. The transformation from low pressure to high pressure is achieved through the valve plate. The cylinder block is subject to unbalanced forces from the low-pressure area and high-pressure area. Therefore, the interface between the cylinder block and valve plate plays an important role in improving the pump's efficiency and lifetime [6].

The pressure transformation in the valve plate will result in a huge variation gradient. In addition, flow passages in the cylinder block are irregular and complex. They exacerbate oil cavitation [7–9]. The pressure of some places in the interface between the cylinder block and valve plate is less than the gas separation pressure. The separated bubbles will be crushed when they arrive at the high-pressure area of the valve plate. Energies released by the bubbles can damage this interface and decrease the volumetric efficiency [10,11].

Numerous studies on the cavitation of axial piston pumps have been carried out. In terms of the analysis of the cavitation mechanism, the centrifugal effect of fluid in the cylinder block can result in pressure differences between the outside wall and inside wall, and the cavitation is more likely to appear in the inside wall [12]. The effect of the fluid temperature on the cavitation is analyzed. The high viscosity caused by the low temperature will aggravate the cavitation [13]. Throttling structures of the valve plate have an important influence on the pressure transformation. An unreasonable structure design causes the pressure variation gradient to increase [14]. Triangular grooves of the spherical valve plate cause special cavitation [15]. Low suction pressure of the inlet will induce insufficient inlet flow [16]. In addition, the effect of a long pipeline for the inlet on wave propagation is investigated [17].

The above-mentioned factors can exacerbate the cavitation problems of axial piston pumps. In order to reduce the intensity of cavitation, methods for improving these factors are proposed. Anti-cavitation throttling structures of the valve plate [18,19], a higher back pressure of the inlet [20,21], an optimized suction duct [22], and an improved unloading outlet [23] are utilized for cavitation suppression. During the analysis of the cavitation mechanism and cavitation suppression, computational fluid dynamics (CFD) models are built. Four CFD models, based on the cavitation [3] and a CFD model based on the full cavitation [22] are proposed for the modelling of pumps' cavitation. A full CFD model is developed from the fluid compressibility, gaseous dynamics, and cavitation damage [24]. The vapor cavitation [25] based CFD model is presented to identify the critical inlet pressure [26]. Apart from the CFD model, an analytical cavitation model is used to determine the pump's speed limitations [27].

For the detection of cavitation for axial piston pumps, the vibration signal is widely used as an indicator for the machine learning model. The denoised time frequency images [28] and multi-channel signals [29] are put into the convolutional neural networks model. Time domain analysis and frequency spectral analysis of the vibration signal are carried out to detect the pumps' cavitation on line [30].

Pumps' cavitation will increase the flow leakage and pressure impact. Therefore, the discharge pressure has a strong correlation with the cavitation, in contrast to the vibration signal [31,32]. In particular, specific cavitation can damage the surface of the cylinder block and valve plate. The specific cavitation damage is shown in Figure 1. This damage is located between the two adjacent piston holes of the cylinder block. It should be pointed out that there is little research on the modelling and fault diagnosis of cavitation damage based on the pressure signal. In addition, the effects of the specific cavitation damage on the discharge pressure are unclear.

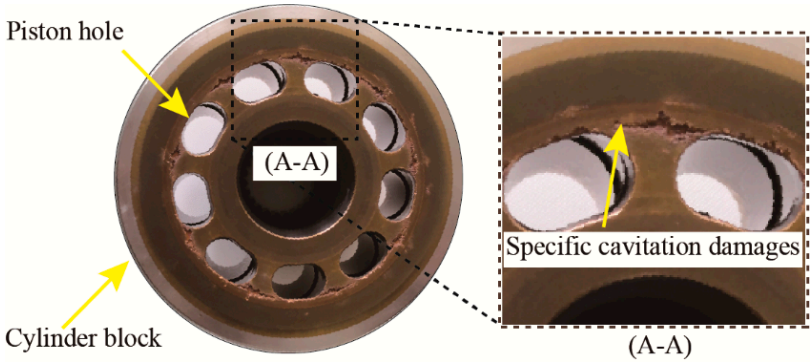

Figure 1. Specific cavitation damage to axial piston pumps.

In this paper, a model of the discharge pressure is built, which takes into account effects of the specific cavitation damage. Fault detection, based on the discharge pressure model, is accomplished. The remainder of this paper is structured as follows. Section 2 describes the simulation model of the pump's discharge pressure. Section 3 presents the

experimental investigation on the cavitation damage. Section 4 shows the results and discussions of the simulation model and experimental investigation. Conclusions are summarized in Section 5.

2. Simulation Model

2.1. Discharge Pressure

The typical structure of an axial piston pump is shown in Figure 2. The pump rotor system mainly includes the shaft, cylinder block, piston, slipper, and retainer. The shaft is supported by the large and small bearings at both ends. The cylinder block is in splined connection with the shaft. Pistons are at equal distance around the cylinder block center. Slippers and pistons are linked by spherical hinges. When the rotor system rotates, pistons reciprocate along the cylinder block hole under the action of the retainer and inclined swash plate. Oil suction and extrusion are accomplished by the pistons' reciprocating motions and valve plate with the high-pressure area and low-pressure area.

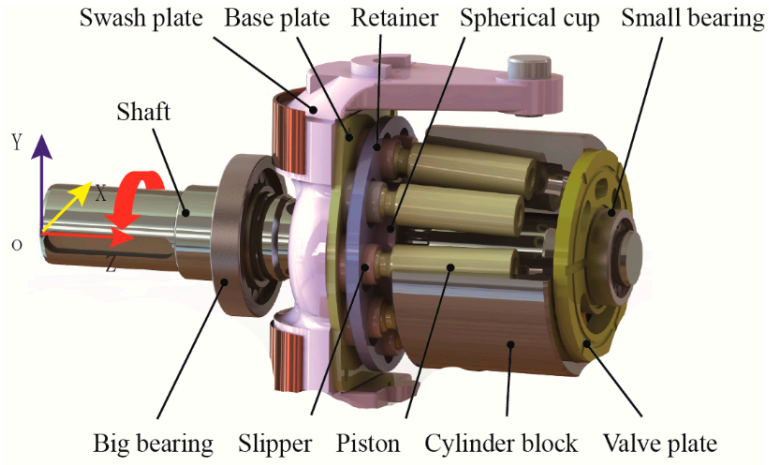

Figure 2. Typical structure of an axial piston pump.

The discharge pressure of an axial piston pump is a key parameter during the oil extrusion process. It depends on the pump's kinematics. The kinematic diagram of the piston pump is shown in Figure 3. The coordinate systems O-xyz and O′-x′y′z′ represent the positions when the inclined angles of the swash plate are 0 and β, respectively. The angle γ is the inclined angle of pistons in the cylinder block hole. The point M′ represents the piston's position when the shaft rotates clockwise by an angle φ. Assuming $OO'' = x_0$, $OM = R$, $O''M_x = x$, $MM' = h$, $MM'' = r$, $MM_z = n$, one can obtain the following equations:

$$h = (x - x_0)/\cos\gamma,\ x = n\tan\beta = (R + r)\tan\beta\cos\varphi,\ r = (x - x_0)\tan\gamma. \quad (1)$$

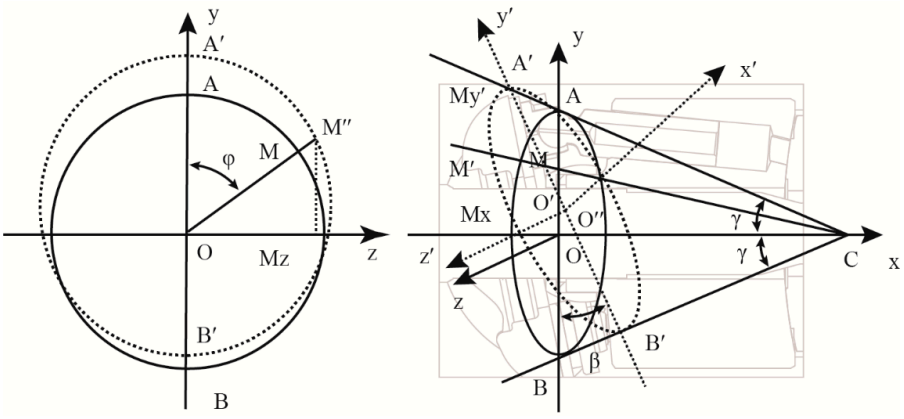

Figure 3. Kinematic diagram of an axial piston pump.

By substituting parameters r and x in the parameter h, one can obtain the following equation:

$$h = \frac{R\tan\beta\cos\varphi - x_0}{\cos\gamma(1-\cos\varphi\tan\beta\tan\gamma)} \tag{2}$$

The piston displacement of the reciprocating motions along the cylinder block hole is calculated as:

$$x_{\mathrm{p}}(1) = \frac{(R - x_0\tan\gamma)\tan\beta(1-\cos\varphi)}{\cos\gamma(1-\tan\beta\tan\gamma)(1-\cos\varphi tan\beta tan\gamma)}, \tag{3}$$

where $x_{\mathrm{p}}(1)$ refers to the piston displacement of the first piston when the shaft rotates clockwise by an angle φ. The piston displacement of the kth piston is $x_{\mathrm{p}}(k)$:

$$x_{\mathrm{p}}(k) = \frac{(R - x_0\tan\gamma)\tan\beta[1-\cos(\varphi+2\pi k/Z)]}{\cos\gamma(1-\tan\beta\tan\gamma)[1-\cos(\varphi+2\pi k/Z)tan\beta tan\gamma]}, \tag{4}$$

where Z is the number of pistons distributed in the cylinder block. The axial piston pump presented in this paper has an odd number of pistons.

The piston velocity of the reciprocating motions along the cylinder block hole is calculated as:

$$\begin{aligned} v_{\mathrm{p}}(1) &= \frac{\mathrm{d}x_{\mathrm{p}}(1)}{\mathrm{d}t} = \frac{\omega_{\mathrm{s}}\sin\varphi\tan\beta(R - x_0\tan\gamma)}{\cos\gamma(1-\cos\varphi\tan\beta\tan\gamma)^2} \\ &\vdots \\ v_{\mathrm{p}}(k) &= \frac{\mathrm{d}x_{\mathrm{p}}(k)}{\mathrm{d}t} = \frac{\omega_{\mathrm{s}}\sin(\varphi+2\pi k/Z)\tan\beta(R - x_0\tan\gamma)}{\cos\gamma[(1-\cos(\varphi+2\pi k/Z)\tan\beta\tan\gamma)]^2} \\ &\vdots \\ v_{\mathrm{p}}(Z) &= \frac{\mathrm{d}x_{\mathrm{p}}(Z)}{\mathrm{d}t} = \frac{\omega_{\mathrm{s}}\sin(\varphi+2\pi)\tan\beta(R - x_0\tan\gamma)}{\cos\gamma[(1-\cos(\varphi+2\pi)\tan\beta\tan\gamma)]^2}, \end{aligned} \tag{5}$$

where ω_{s} is the rotating speed of the cylinder block.

The output flow rate of an axial piston pump depends on the flow of a single piston located in the high-pressure area. The flow of the kth piston is calculated as:

$$Q_{\mathrm{p}}(k) = \pi r_{\mathrm{p}}^2 v_{\mathrm{p}}(k) - Q_{\mathrm{c1}}(k) - Q_{\mathrm{c2}}(k) - Q_{\mathrm{c3}}(k), \tag{6}$$

where r_{p} refers to the radius of the piston. $Q_{\mathrm{c1}}(k)$, $Q_{\mathrm{c2}}(k)$, and $Q_{\mathrm{c3}}(k)$ are leakage flows of the slipper pair, the piston pair, and the valve plate pair, respectively.

$$Q_{\mathrm{c1}}(k) = \frac{\pi h_{\mathrm{c1}}^3\lambda\left[P_{\mathrm{p}}(k) - P_{\mathrm{le}}\right]}{6\mu(\ln r_{\mathrm{s}} - \ln R_{\mathrm{s}})}, \tag{7}$$

where h_{c1} is the clearance between the slipper and a base plate. λ refers to the pressure ratio coefficient. $P_{\mathrm{p}}(k)$ represents the pressure of the kth piston. P_{le} is the pressure of the leakage port. μ refers to the dynamic viscosity. r_{s} and R_{s} are radius of the sealing belt for slippers.

$$Q_{\mathrm{c2}}(k) = \frac{2\pi r_{\mathrm{p}}h_{c2}^3 + 3\varepsilon^2\pi r_{\mathrm{p}}h_{c2}^3}{12\mu l_{\mathrm{p}}}\left[P_{\mathrm{p}}(k) - P_{\mathrm{le}}\right], \tag{8}$$

where h_{c2} and l_{p} represent the clearance and contact length between the piston and cylinder block, respectively. ε refers to the eccentricity.

$$Q_{\mathrm{c3}}(k) = \frac{\pi\lambda h_{\mathrm{c3}}^3}{6\mu}\left(\frac{\varphi_2 - \varphi_1}{\ln R_2 - \ln R_1} + \frac{\varphi_2 - \varphi_1}{\ln R_4 - \ln R_3}\right)\left[P_{\mathrm{p}}(k) - P_{\mathrm{le}}\right], \tag{9}$$

where h_{c3} is the clearance between the cylinder block and a valve plate. R_1, R_2, R_3, and R_4 represent the radius of the sealing belt for the valve plate. φ_1 and φ_2 are the distribution angles of the damping grooves.

The output flow rate Q_{out} is the sum of instantaneous flows of pistons distributed in the high-pressure area:

$$\begin{aligned} Q_{\text{out}} &= Q_{\text{p}}(1) + Q_{\text{p}}(2) + \cdots + Q_{\text{p}}(K) \\ &= \pi r_{\text{p}}^2 \sum_1^K v_{\text{p}}(k) + \sum_1^K Q_{\text{c1}}(k) - \sum_1^K Q_{\text{c2}}(k) - \sum_1^K Q_{\text{c3}}(k), \end{aligned} \tag{10}$$

where the number K of pistons distributed in the high-pressure area is calculated as:

$$K = \begin{cases} \frac{Z+1}{2} & 0 < \varphi \le \frac{\pi}{Z} \\ \frac{Z-1}{2} & \frac{\pi}{Z} < \varphi \le \frac{2\pi}{Z}. \end{cases} \tag{11}$$

The time derivative of the discharge pressure P_{out} is given by:

$$\begin{aligned} \frac{dP_{\text{out}}}{dt} &= \frac{Q_{\text{out}} B_{\text{f}}}{V_{\text{out}}} \\ &= \frac{\pi r_{\text{p}}^2 B_{\text{f}}}{V_{\text{out}}} \sum_1^K v_{\text{p}}(k) + \frac{B_{\text{f}}}{V_{\text{out}}} \sum_1^K Q_{\text{c1}}(k) - \frac{B_{\text{f}}}{V_{\text{out}}} \sum_1^K Q_{\text{c2}}(k) - \frac{B_{\text{f}}}{V_{\text{out}}} \sum_1^K Q_{\text{c3}}(k), \end{aligned} \tag{12}$$

where B_{f} is the fluid bulk modulus. V_{out} refers to the volume of the output port.

The time derivative of the pressure $P_{\text{p}}(k)$ for the kth piston is calculated as:

$$\begin{aligned} \frac{dP_{\text{p}}(k)}{dt} &= \frac{Q_{\text{p}}(k) B_{\text{f}}}{V(k)} \\ &= \frac{\pi r_{\text{p}}^2 B_{\text{f}}}{V(k)} v_{\text{p}}(k) - \frac{B_{\text{f}}}{V(k)} Q_{\text{c1}}(k) - \frac{B_{\text{f}}}{V(k)} Q_{\text{c2}}(k) - \frac{B_{\text{f}}}{V(k)} Q_{\text{c3}}(k), \end{aligned} \tag{13}$$

where $V(k)$ refers to the volume of the kth piston.

2.2. Input of the Specific Cavitation Damage

As shown in Figure 1, the specific cavitation damage will lead to internal leakage flows between the adjacent pistons [33]. The size of the cavitation damage is approximately a slender hole. Therefore, the flow model of the slender hole is utilized as an input of the specific cavitation damage in the discharge pressure model. It is assumed that a specific cavitation damage is located between the kth piston and $k+1$th piston. The leakage flow of the specific cavitation damage Q_{scd} is given by the flow model of the slender hole:

$$Q_{\text{scd}} = \frac{\pi d_{\text{scd}}^3 \left[P_{\text{p-scd}}(k) - P_{\text{p-scd}}(k+1) \right]}{128 \mu l_{\text{scd}}}, \tag{14}$$

where d_{scd} and l_{scd} are the diameter and length of the slender hole, respectively. $P_{\text{p-scd}}(k)$ and $P_{\text{p-scd}}(k+1)$ represent the pressures of the kth piston and $k+1$th piston with the input of the specific cavitation damage. The flows of the adjacent pistons are given by the following equations:

$$Q_{\text{p-scd}}(k) = \pi r_{\text{p}}^2 v_{\text{p}}(k) - Q_{\text{c1}}(k) - Q_{\text{c2}}(k) - Q_{\text{c3}}(k) - Q_{\text{scd}} \tag{15}$$

$$Q_{\text{p-scd}}(k+1) = \pi r_{\text{p}}^2 v_{\text{p}}(k+1) - Q_{\text{c1}}(k+1) - Q_{\text{c2}}(k+1) - Q_{\text{c3}}(k+1) + Q_{\text{scd}}. \tag{16}$$

The output flow rate $Q_{\text{out-scd}}$ with the input of the specific cavitation damage is the difference between the output flow rate Q_{out} and the internal leakage flow Q_{scd}:

$$\begin{aligned} Q_{\text{out-scd}} &= Q_{\text{p}}(1) + Q_{\text{p}}(2) + \cdots + Q_{\text{p}}(K) - Q_{\text{scd}} \\ &= \pi r_{\text{p}}^2 \sum_1^K v_{\text{p}}(k) + \sum_1^K Q_{\text{c1}}(k) - \sum_1^K Q_{\text{c2}}(k) - \sum_1^K Q_{\text{c3}}(k) - Q_{\text{scd}}. \end{aligned} \tag{17}$$

The time derivative of the discharge pressure $P_{\text{out-scd}}$ with the input of the specific cavitation damage is given by:

$$\begin{aligned}\frac{dP_{\text{out-scd}}}{dt} &= \frac{Q_{\text{out-scd}}B_{\text{f}}}{V_{\text{out}}} \\ &= \frac{\pi r_{\text{p}}^2 B_{\text{f}}}{V_{\text{out}}}\sum_{1}^{K} v_{\text{p}}(k) + \frac{B_{\text{f}}}{V_{\text{out}}}\sum_{1}^{K} Q_{\text{c1}}(k) - \frac{B_{\text{f}}}{V_{\text{out}}}\sum_{1}^{K} Q_{\text{c2}}(k) - \\ &\frac{B_{\text{f}}}{V_{\text{out}}}\sum_{1}^{K} Q_{\text{c3}}(k) - \frac{B_{\text{f}}Q_{\text{scd}}}{V_{\text{out}}}.\end{aligned} \tag{18}$$

The time derivative of the pressures $P_{\text{p-scd}}(k)$ and $P_{\text{p-scd}}(k+1)$ for the kth piston and mboxemphk + 1th piston is calculated as:

$$\begin{aligned}\frac{dP_{\text{p-scd}}(k)}{dt} &= \frac{Q_{\text{p-scd}}(k)B_{\text{f}}}{V(k)} \\ &= \frac{\pi r_{\text{p}}^2 B_{\text{f}} v_{\text{p}}(k)}{V(k)} - \frac{B_{\text{f}}Q_{\text{c1}}(k)}{V(k)} - \frac{B_{\text{f}}Q_{\text{c2}}(k)}{V(k)} - \\ &\frac{B_{\text{f}}Q_{\text{c3}}(k)}{V(k)} - \frac{B_{\text{f}}Q_{\text{scd}}}{V(k)}\end{aligned} \tag{19}$$

$$\begin{aligned}\frac{dP_{\text{p-scd}}(k+1)}{dt} &= \frac{Q_{\text{p-scd}}(k+1)B_{\text{f}}}{V(k+1)} \\ &= \frac{\pi r_{\text{p}}^2 B_{\text{f}} v_{\text{p}}(k+1)}{V(k+1)} - \frac{B_{\text{f}}Q_{\text{c1}}(k+1)}{V(k+1)} - \frac{B_{\text{f}}Q_{\text{c2}}(k+1)}{V(k+1)} - \\ &\frac{B_{\text{f}}Q_{\text{c3}}(k+1)}{V(k+1)} + \frac{B_{\text{f}}Q_{\text{scd}}}{V(k+1)}.\end{aligned} \tag{20}$$

2.3. Model Properties

Simulation models with the specific cavitation damage are constructed based on the flow continuity and pressure derivative equation. The main parameters of the pump simulation models are listed in Table 1.

Table 1. Simulation model properties.

Parameters	Values	Parameters	Values
γ	5°	β	14°
R	36.75 mm	Z	9
ω_s	1500 r/min	r_{p}	8.50 mm
h_{c1}	0.01 mm	x_0	8.89 mm
P_{le}	0.10 MPa	λ	0.9
r_{s}	7.70 mm	μ	46 cP
h_{c2}	0.02 mm	R_{s}	9.10 mm
h_{c3}	0.01 mm	ε	0.01 mm
R_2	23.50 mm	R_1	20.00 mm
R_4	34.75 mm	R_3	31.50 mm
φ_2	154°	φ_1	26°
V_{out}	48.60 mm^3	B_f	1.7×10^{-2} MPa
d_{scd}	0.5 mm/0.8 mm	l_{scd}	6.0 mm

The normal pump model and simulation models with specific cavitation damage input (case 1: d_{scd} = 0.5 mm, case 2: d_{scd} = 0.8 mm) are constructed. The rotating speed of the cylinder block is 1500 r/min. The initial pressure of the discharge pressure is 21.0 MPa. The simulation models are solved through the Runge–Kutta numerical integration algorithm. The fixed time step valve is 1×10^{-4} s. The order of the integration algorithm is 4. The total simulation time is 0.2 s.

3. Experimental Investigation

3.1. Layout of the Test Rig

Experimental investigation on the axial piston pump was carried out. The test rig of the pump is shown in Figure 4a. The system schematic diagram of this test rig is

presented in Figure 4b. The power of the electric motor as supplied to the pump through the torque-speed sensor. The pump converted mechanical energy into fluid power. The discharge pressure of the pump was measured through the pressure gauge and pressure sensor. A relief valve was used as the regulator of the discharge pressure. A flow sensor was placed between the pump and relief valve. Detailed descriptions of the test rig are shown in Table 2.

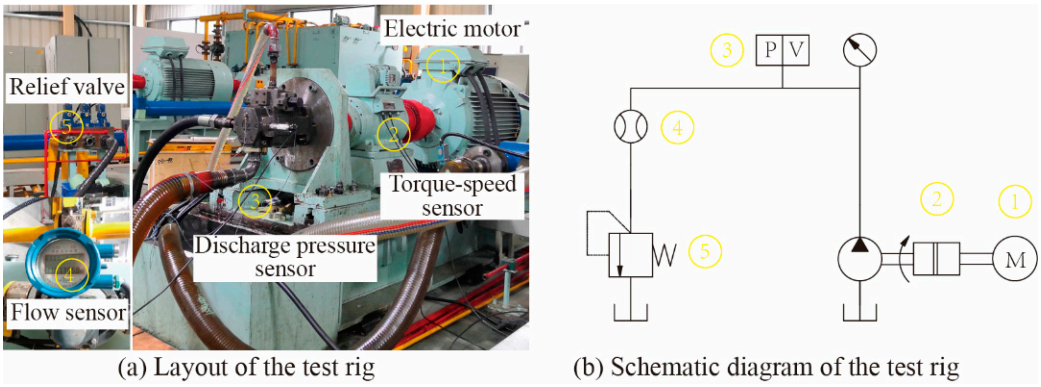

Figure 4. Layout and schematic diagram of the test rig.

Table 2. Detailed descriptions of the test rig.

No.	Components	Descriptions
1	Electric motor	ABB-IEL-280M75
2	Torque-speed sensor	ZJ-5000/3000-120-02
3	Discharge pressure sensor	HM90-0~35MPa-H3V2F1
4	Flow sensor	LXB-1
5	Relief valve	DBW30B-1-50B/350

3.2. Testing Pump with Cavitation Damage

The valve plate pair of the testing pump is shown in Figure 5. Specific cavitation damage was applied between the adjacent piston holes of the cylinder block. The size of the specific damage was 6.0 mm × 2.0 mm × 1.0 mm. An axial piston pump with specific cavitation damage and a normal pump was tested on the test rig. The motor speed was 1500 r/min. The discharge pressure was regulated at around 21.0 MPa. All the pumps had full displacements. The discharge pressures of the tested pumps were measured for 10 s with a sampling frequency of 48,000 Hz.

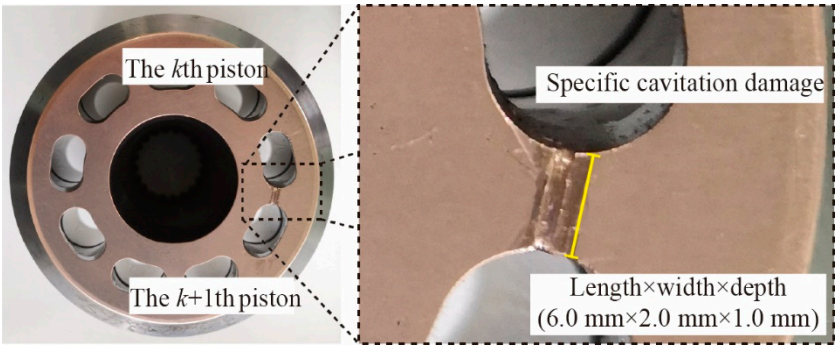

Figure 5. Valve plate pair with specific cavitation damage.

4. Results and Discussion

4.1. Simulations

The discharge pressure of the simulation model with no specific cavitation damage is shown in Figure 6. It can be seen that the pressure oscillation is due to the iterative calculation during the initial stage. The discharge pressure becomes convergent after 6.5×10^{-4} s. The pressure cure fluctuates around 21.0 MPa. The fluctuation range is ± 0.2 MPa. This means that the simulation model is effectively solved through the numerical integration.

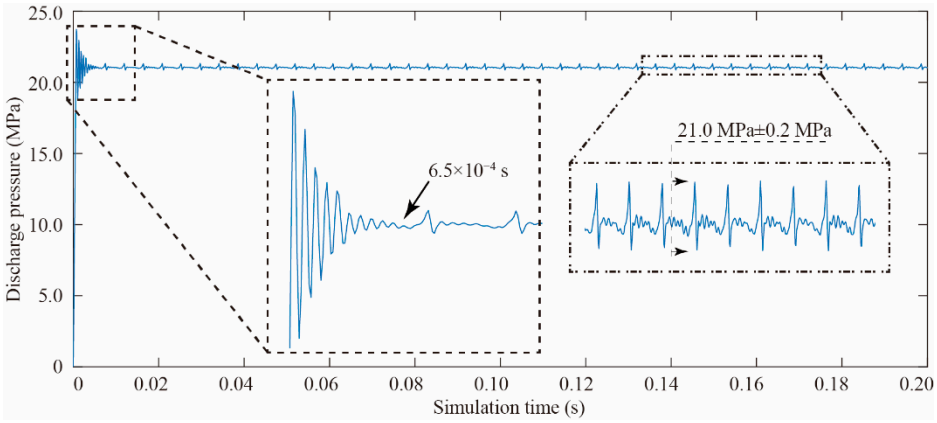

Figure 6. Simulated discharge pressure during the iterative process (normal pump model, rotational speed: 1500 r/min, discharge pressure: 21 MPa).

Discharge pressures of the normal pump model and pump models with specific cavitation damage (case 1: 0.5 mm, case 2: 0.8 mm) are shown in Figure 7. Considering that the discharge pressure fluctuates periodically, pressures under different model cases are compared during two cycles (0.08 s). It can be seen that the pressure curve of case 1 has nearly uniform spikes. There are a lot of signal burrs in case 1 and case 2. The burrs occur at 0 s, 0.2 s, 0.4 s, 0.6 s, and 0.8 s. In addition, the amplitudes of burrs in case 2 are higher than those in case 1. The results show that specific cavitation damages in the valve plate pair cause the discharge pressure to become distorted. On average, there are two signal distortions in a cycle. The greater the damage, the greater the signal distortion.

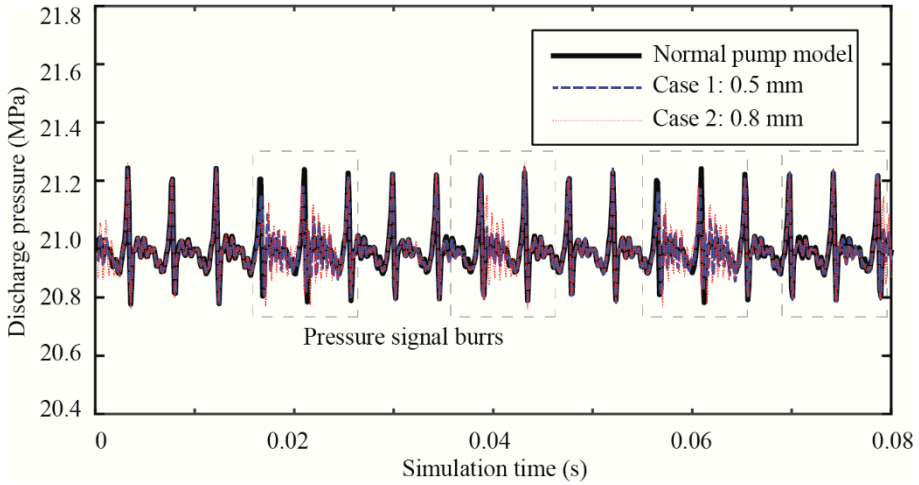

Figure 7. Comparisons of the simulated discharge pressures under different model cases.

Spectra of the discharge pressures under three cases are shown in Figure 8. The spectral energy of the pressure is mainly concentrated in the 1st, 2nd, 3rd, and 4th pumping

frequencies. The amplitudes of these frequencies for case 1 and case 2 are lower than those in the normal pump model. In addition, the amplitudes in case 2 are less than the amplitudes in case 1. This shows that specific cavitation damage will decrease the amplitudes of the pumping frequencies in the spectra. As the damage increases, the amplitudes become smaller. The spectral energies of the pumping frequencies in case 1 and case 2 are allocated to other sidebands around themselves. It can be seen that the spectrum of the normal pump model has almost no 25 Hz sideband, while the amplitudes of this sideband for case 1 and case 2 increase gradually. In addition, amplitudes of the sideband around the 4th pumping frequency are larger than those around the 2nd and 3rd pumping frequency. No sideband can be found around the 1st pumping frequency. Moreover, the spectra of case 1 and case 2 have frequencies (50 Hz, 100 Hz, 150 Hz, and 200 Hz) below the 1st pump frequency. The amplitudes of these frequencies increase as damage increases.

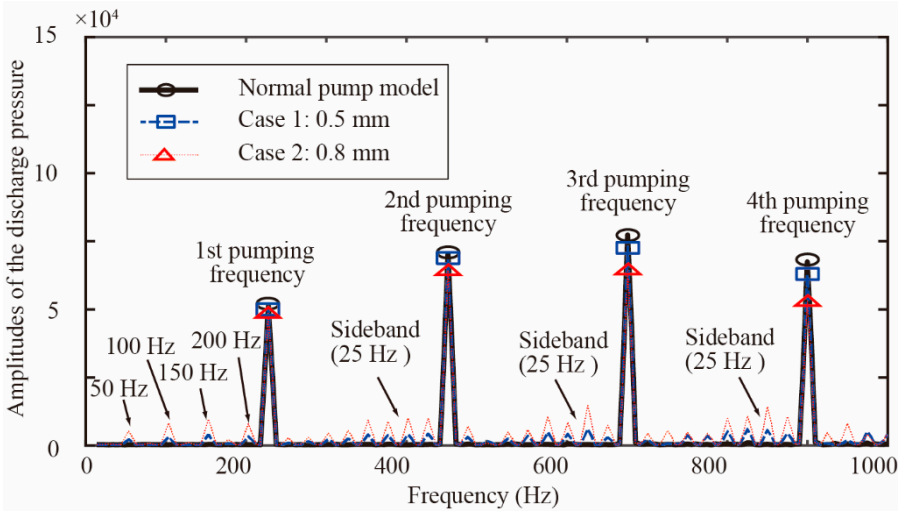

Figure 8. Spectra of the discharge pressures under different model cases.

Comparisons of the simulated discharge pressures and their spectra show that the specific cavitation damage will lead to waveform distortions, spectrum energy relocation, and the generation of new frequencies and sidebands. In order to study the effects of these influence mechanisms on the discharge pressure, internal leakage flow rates of the slender hole are shown in Figure 9. We define the flow rates as positive flows and negative flows. Positive flow occurs when the pressure of the k + 1th piston is larger than the pressure of the kth piston. In the opposite case, it is called negative flow. It can be seen that flow rates alternately appear at 0 s, 0.2 s, 0.4 s, 0.6 s, and 0.8 s. The absolute values of flow rates for case 1 and case 2 are 1.83 L/min and 4.69 L/min, respectively. This means that high specific damage will lead to more leakage flows between the adjacent pistons. In addition, backflows occur at the start and end of the positive flows and negative flows. The specific cavitation damage in the valve plate pair exacerbates the backflows in axial piston pumps. Backflows in case 2 are higher than those in case 1. The maximum backflows of case 1 and case 2 are −0.91 L/min and −0.40 L/min, respectively.

The internal pressures of the kth piston and k + 1th piston are shown in Figure 10. The initial pressures in the kth piston and k + 1th piston are the inlet pressures (0.1 MPa) due to the fact that two pistons are located in the low-pressure area. The pressure of the kth piston and the k + 1th piston becomes the discharge pressure (21.0 MPa) when the shaft rotates by an angle of $2\pi(k-1)/Z$ and $2\pi k/Z$, respectively. At this time, backflows appear, and the pressure difference results in the negative flow rate. Then, the two adjacent pistons are both located in the high-pressure area and no flow is found with no pressure difference. Positive flow rates appear when the pressure of the kth piston becomes the inlet pressure. It is also found that the amplitudes of the pressure spikes decrease when the pump has specific cavitation. The maximum pressure spikes for the normal pump model, case 1 and case

2 are 23.0 MPa, 22.6 MPa and 22.1 MPa, respectively. The results show that the pressure difference between the two adjacent pistons leads to leakage flow and discharge pressure distortions of axial piston pumps.

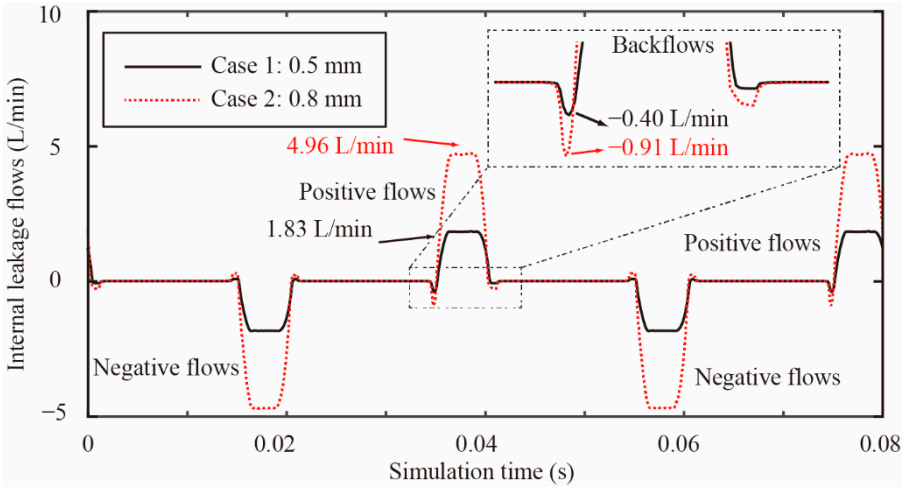

Figure 9. Internal leakage flows of the slender hole.

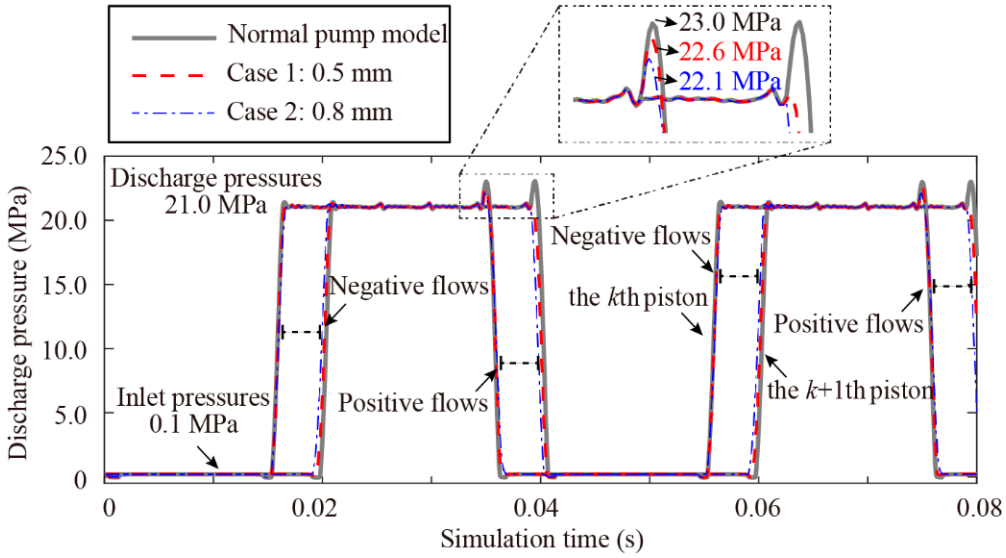

Figure 10. Internal pressures of the *k*th piston and the *k* + 1th piston.

4.2. Cavitation Damage Detection

The experimental results of discharge pressures for the normal pump and the testing pump with cavitation damage are shown in Figure 11. Measured discharge pressures during the two cycles are shown in Figure 11a. The tested pressure of the normal pump fluctuates around 21.0 MPa. It ranges from 20.8 MPa to 21.2 MPa. The variations of the tested pressures are consistent with the simulation results shown in Figure 7. Some signal distortions of the tested pressure for the testing pump with cavitation damage are found at 0.2 s and 0.4 s during one cycle. This is because internal leakage flows appear in the corresponding time due to the specific cavitation damages, as shown in Figure 9.

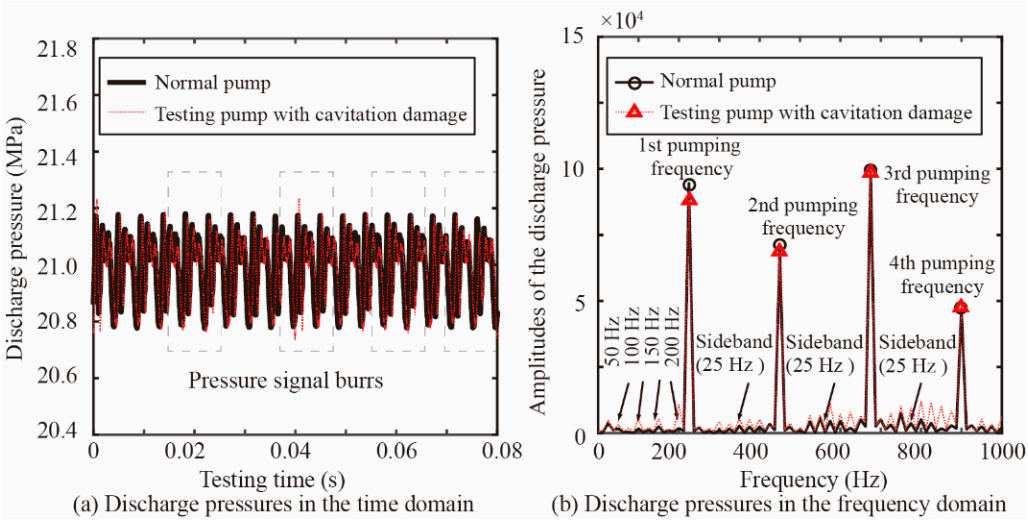

Figure 11. Comparisons of the tested discharge pressures and their spectra.

Frequency spectra of the tested discharge pressures for the normal pump and the testing pump with cavitation damage are shown in Figure 11b. Spectral energies are mostly located in the first four pumping frequencies. The 3rd pumping frequency has the maximum amplitudes. It can be seen that the specific cavitation damage results in amplitude decreases for these pumping frequencies. Sidebands with a frequency of 25 Hz appear in the spectra. In particular, the amplitudes of the sideband around the 4th pumping frequency are larger than the sidebands around the 2nd and 3rd pumping frequency. In addition, the 50 Hz frequency and its harmonics also occur below the 1st pumping frequency. The experimental results show that the waveform distortions, spectrum energy relocation, and the generation of new frequencies and sidebands can be used as features for the fault detection of the specific cavitation damage of axial piston pumps.

5. Conclusions

This paper proposes a discharge pressure-based model and a fault detection methodology for the specific cavitation damage of axial piston pumps. A slender hole is used as the input of the simulated discharge pressure model with specific damage. An experimental investigation on the fault detection of cavitation damage is carried out. The following conclusions are drawn. First, the modelling methodology based on the pressure and slender hole is applicable for the cavitation damage detection. Second, the internal leakage flow leads to waveform distortions of the adjacent piston pressure and discharge pressure. Third, specific cavitation damage gives rise to new frequency of 50 Hz and its harmonics, 25 Hz sidebands around the 4th pumping frequency. These frequencies and sidebands in the spectra can be used as fault features for the specific cavitation damage detection of axial piston pumps.

Author Contributions: Conceptualization, S.X. and Y.X.; methodology, S.X.; software, S.X.; validation, S.X., Y.X. and J.X.; formal analysis, S.X.; investigation, S.X.; resources, Y.X.; data curation, S.X.; writing—original draft preparation, S.X.; writing—review and editing, S.X.; visualization, S.X.; supervision, Y.X.; project administration, J.X.; funding acquisition, Y.X. All authors have read and agreed to the published version of the manuscript.

Funding: This research was funded by the National Key Research and Development Program of China (Grant No. 2020YFB2007101), the Project of State Key Laboratory of High Performance Complex Manufacturing (Grant No. ZZYJKT2021-16), and the Open Foundation of the State Key Laboratory of Fluid Power and Mechatronic Systems (Grant No. GZKF-202007).

Institutional Review Board Statement: Not applicable.

Informed Consent Statement: Not applicable.

Data Availability Statement: The data presented in this study are available on request from the corresponding author. The data are not publicly available due to an ongoing study.

Acknowledgments: The authors would like to thank the following people: Zhihua Ye, Huaijun Shi and Ping Wu in Ningbo Hilead Hydraulic Co., Ltd., for their help in preparing the pumps and performing the tests.

Conflicts of Interest: The authors declare no conflict of interest.

References

1. Suh, S.; Kim, W. Nonlinear Position Control Using Differential Flatness Concept with Load Torque Observer for Electro Hydraulic Actuators with Sinusoidal Load Torque. *Mathematics* **2020**, *8*, 1484. [CrossRef]
2. Xu, H.G.; Zhang, J.H.; Sun, G.M.; Huang, W.D.; Huang, X.C.; Lyu, F.; Xu, B.; Su, Q. The direct measurement of the cylinder block dynamic characteristics based on a non-contact method in an axial piston pump. *Measurement* **2021**, *167*, 108279. [CrossRef]
3. Casoli, P.; Vacca, A.; Franzoni, G.; Berta, G.L. Modelling of fluid properties in hydraulic positive displacement machines. *Simul. Model. Pract. Theory* **2006**, *14*, 1059–1072. [CrossRef]
4. He, Y.; Tang, H.; Ren, Y.; Kumar, A. A deep multi-signal fusion adversarial model based transfer learning and residual network for axial piston pump fault diagnosis. *Measurement* **2022**, *192*, 110889. [CrossRef]
5. Chao, Q.; Zhang, J.; Xu, B.; Wang, Q. Multi-position measurement of oil film thickness within the slipper bearing in axial piston pumps. *Measurement* **2018**, *122*, 66–72. [CrossRef]
6. Richardson, D.; Sadeghi, F.; Rateick, R.G.; Rowan, S. Experimental and Analytical Investigation of Floating Valve Plate Motion in an Axial Piston Pump. *Tribol. Trans.* **2017**, *60*, 537–547. [CrossRef]
7. Zhang, C.C.; Zhu, C.H.; Meng, B.; Li, S. Challenges and Solutions for High-Speed Aviation Piston Pumps: A Review. *Aerospace* **2021**, *8*, 392. [CrossRef]
8. Brijkishore; Khare, R.; Prasad, V. Prediction of cavitation and its mitigation techniques in hydraulic turbines-A review. *Ocean Eng.* **2021**, *221*, 108512. [CrossRef]
9. Wang, X.; Zhou, S.; Shan, Z.; Yin, M. Investigation of Cavitation Bubble Dynamics Considering Pressure Fluctuation Induced by Slap Forces. *Mathematics* **2021**, *9*, 2064. [CrossRef]
10. Yun, L.; Yan, Z.; Jianping, C.; Rongsheng, Z.; Dezhong, W. A cavitation performance prediction method for pumps: Part2-sensitivity and accuracy. *Nucl. Eng. Technol.* **2021**, *53*, 3612–3624. [CrossRef]
11. Osterland, S.; Muller, L.; Weber, J. Influence of Air Dissolved in Hydraulic Oil on Cavitation Erosion. *Int. J. Fluid Power* **2021**, *22*, 373–392. [CrossRef]
12. Chao, Q.; Zhang, J.H.; Xu, B.; Huang, H.P.; Zhai, J. Centrifugal effects on cavitation in the cylinder chambers for high-speed axial piston pumps. *Meccanica* **2019**, *54*, 815–829. [CrossRef]
13. Chao, Q.; Xu, Z.; Tao, J.F.; Liu, C.L.; Zhai, J. Cavitation in a high-speed aviation axial piston pump over a wide range of fluid temperatures. *Proc. Inst. Mech. Eng. Part A J. Power Energy* **2021**, *236*, 727–737. [CrossRef]
14. Sun, Z.G.; Li, Y.D.; Liang, N.; Zhong, H.M. Study on Restraining Cavitation of Axial Piston Pump Based on Structure of Cylinder Block and Valve Plate Triangular Throttling Groove. *Shock Vib.* **2022**, *1*, 6918936.
15. Zhao, B.; Guo, W.W.; Quan, L. Cavitation of a Submerged Jet at the Spherical Valve Plate/Cylinder Block Interface for Axial Piston Pump. *Chin. J. Mech. Eng.* **2020**, *33*, 67. [CrossRef]
16. Sachdeva, A.; Borkar, K.; Bhansali, A.; Salutagi, S. Critical Inlet Pressure Prediction for Inline Piston Pumps Using Multiphase Computational Fluid Dynamics Modelling. *SAE Int. J. Aerosp.* **2021**, *14*, 117–126. [CrossRef]
17. Manhartsgruber, B. Non-linear dynamics of a hydraulic piston pump model with long suction line and cavitation. In Proceedings of the International Workshop on Power Transmission and Motion Control, Bath, UK, 15 August 2003.
18. Shi, Y.X.; Lin, T.R.; Meng, G.Y.; Huang, J.X. A Study on the Suppression of Cavitation Flow Inside an Axial Piston Pump. In Proceedings of the Prognostics and System Health Management Conference, Chengdu, China, 19 January 2017.
19. Ye, S.G.; Zhang, J.H.; Xu, B.; Song, W.; Chen, L.; Shi, H.Y.; Zhu, S.Q. Experimental and numerical studies on erosion damage in damping holes on the valve plate of an axial piston pump. *J. Mech. Sci. Technol.* **2017**, *31*, 4285–4295. [CrossRef]
20. Lu, L.; Fu, X.; Ryu, S.; Yin, Y.B.; Shen, Z.X. Comprehensive discussions on higher back pressure system performance with cavitation suppression using high back pressure. *Proc. Inst. Mech. Eng. Part C J. Mech. Eng. Sci.* **2018**, *233*, 2442–2455. [CrossRef]
21. Manhartsgruber, B. A novel concept for boosting the suction line of piston pumps by piezo-actuated pipe walls. In Proceedings of the Bath/Asme Symposium on Fluid Power and Motion Control, Bath, UK, 12 September 2018.
22. Fang, Y.; Zhang, J.H.; Xu, B.; Mao, Z.B.; Li, C.M.; Huang, C.S.; Lyu, F.; Guo, Z.M. Raising the Speed Limit of Axial Piston Pumps by Optimizing the Suction Duct. *Chin. J. Mech. Eng.* **2021**, *34*, 105–117. [CrossRef]
23. Zhang, B.; Zhao, C.X.; Hong, H.C.; Cheng, G.Z.; Yang, H.Y.; Feng, S.B.; Zhai, J.; Xiao, W.H. Optimization of the outlet unloading structure to prevent gaseous cavitation in a high-pressure axial piston pump. *Proc. Inst. Mech. Eng. Part C J. Mech. Eng. Sci.* **2022**, *236*, 3459–3473. [CrossRef]
24. Yin, F.L.; Nie, S.L.; Xiao, S.H.; Hou, W. Numerical and experimental study of cavitation performance in sea water hydraulic axial piston pump. *Proc. Inst. Mech. Eng. Part I J. Syst. Control. Eng.* **2016**, *230*, 716–735. [CrossRef]

25. Jablonska, J.; Kozubkova, M.; Mahdal, M.; Marcalik, P.; Tuma, J.; Bojko, M.; Hruzik, L. Spectral analysis of gaseous cavitation in water through multiphase mathematical and acoustic methods. *Phys. Fluids* **2021**, *33*, 085128. [CrossRef]
26. Dong, H.K.; Wang, Y.; Chen, J.H. First attempt to determine the critical inlet pressure for aircraft pumps with a numerical approach that considers vapor cavitation and air aeration. *Proc. Inst. Mech. Eng. Part G J. Aerosp. Eng.* **2020**, *234*, 1926–1938. [CrossRef]
27. Chao, Q.; Tao, J.F.; Lei, J.B.; Wei, X.L.; Liu, C.L.; Wang, Y.H.; Meng, L.H. Fast scaling approach based on cavitation conditions to estimate the speed limitation for axial piston pump design. *Front. Mech. Eng.* **2021**, *16*, 176–185. [CrossRef]
28. Chao, Q.; Wei, X.; Lei, J.; Tao, J.; Liu, C. Improving accuracy of cavitation severity recognition in axial piston pumps by denoising time–frequency images. *Meas. Sci. Technol.* **2022**, *33*, 055116. [CrossRef]
29. Chao, Q.; Tao, J.F.; Wei, X.L.; Wang, Y.H.; Meng, L.H.; Liu, C.L. Cavitation intensity recognition for high-speed axial piston pumps using 1-D convolutional neural networks with multi-channel inputs of vibration signals. *Alex. Eng. J.* **2020**, *59*, 4463–4473. [CrossRef]
30. Siano, D.; Panza, M.A. Diagnostic method by using vibration analysis for pump fault detection. *Energy Procedia* **2018**, *148*, 10–17. [CrossRef]
31. Zhai, J.; Zhou, H. Model and Simulation on Flow and Pressure Characteristics of Axial Piston Pump for Seawater Desalination. In Proceedings of the International Conference on Mechatronics and Applied Mechanics, Hong Kong, China, 27 December 2011.
32. Guo, M.; Liu, C.; Liu, S.Q.; Ke, Z.F.; Wei, W.; Yan, Q.D.; Khoo, B.C. Detection and evaluation of cavitation in the stator of a torque converter using pressure measurement. *Phys. Fluids* **2022**, *34*, 045124. [CrossRef]
33. Xia, S.; Zhang, J.; Ye, S.; Xu, B.; Xiang, J.; Tang, H. A mechanical fault detection strategy based on the doubly iterative empirical mode decomposition. *Appl. Acoust.* **2019**, *155*, 346–357. [CrossRef]